Protein J (2012) 31:598–608
DOI 10.1007/s10930-012-9436-3

Bovine Carbonyl Lactoperoxidase Structure at 2.0Å Resolution and Infrared Spectra as a Function of pH

Amit K. Singh · Michael L. Smith · Shavait Yamini · Per-Ingvar Ohlsson · Mau Sinha · Punit Kaur · Sujata Sharma · Jan A. K. Paul · Tej P. Singh · K.-G. Paul

Published online: 11 August 2012
© Springer Science+Business Media, LLC 2012

Abstract Lactoperoxidase (LPO) is a hemeprotein catalyzing the oxidation of thiocyanate and I^- into antimicrobials and small aromatic organics after being itself oxidized by H_2O_2. LPO is excreted by the lungs, mammary glands, found in saliva and tears and protects mammals against bacterial, fungal and viral invasion. The Fe(II) form binds CO which inactivates LPO like many other hemeproteins. We present the 3-dimensional structure of CO–LPO at 2.0Å resolution and infrared (IR) spectra of the iron-bound CO stretch from pH 3 to 8.8 at 1 cm^{-1} resolution. The observed Fe–C–O bond angle of 132° is more acute than the electronically related Fe(III), CN–LPO with a Fe–C–N angle of 161°. The orientations of the two ligands are different with the oxygen of CO pointing towards the imidazole of distal His109 while the nitrogen of CN points away, the Fe(II) moves towards His109 while the Fe(III) moves away; both movements are consistent with a hydrogen bond between the distal His109 and CO, but not to the nitrogen of CN–LPO. The IR spectra of CO–LPO exhibit two major CO absorbances with pH dependent relative intensities. Both crystallographic and IR data suggest proton donation to the CO oxygen by His109 with a pK $\approx$ 4; close to the pH of greatest enzyme turnover. The IR absorbance maxima are consistent with a first order correlation between frequency and Fe(III)/Fe(II) reduction potential at pH 7; both band widths at half-height correlate with electron density donation from Fe(II) to CO as gauged by the reduction potential.

Keywords Antimicrobial activity · Lactoperoxidase · Carbon monoxide · Heme · Peroxidase · Protein structure

Abbreviations

ABTS	2,2′-azino-*bis*-(3-ethylbenzthiazoline-6-sulfonic acid)
B-factor	Relative vibrational motion
Cyt c PO	Cytochrome c peroxidase
EPO	Eosinophilperoxidase
FTIR	Fourier transform infrared
G-factor	Overall structure normality
Hb	Hemoglobin
HRP	Horseradish peroxidase
IR	Infrared
LPO	Lactoperoxidase
Mb	Myoglobin
MPO	Myeloperoxidase
PDB	Protein data bank
PEG	Polyethyleneglycol
R factor	Reliability factor
RMSD	Root mean standard deviation
RR	Resonance Raman
TPO	Thyroid peroxidase

A. K. Singh · S. Yamini · M. Sinha · P. Kaur · S. Sharma · T. P. Singh
Department of Biophysics, All India Institute of Medical Sciences, New Delhi 110 029, India
e-mail: aksaiims@gmail.com

T. P. Singh
e-mail: tpsingh.aiims@gmail.com

M. L. Smith (✉)
Jannek Fuel Inc, Mesa, AZ 85206, USA
e-mail: mike@jannekfuel.com

P.-I. Ohlsson · K.-G. Paul
Medical Chemistry, Umeå University, 901 87 Umeå, Sweden

J. A. K. Paul
Jannek Fuel Inc, 162 53 Vællingby, Sweden

1 Introduction

Lactoperoxidase (LPO) is a mammalian enzyme of the protein class(EC 1.11.1.7) which catalyzes the 2-electron oxidation by H_2O_2 of substrates such as reduced halides, SCN^- and small organic molecules. It is closely related to important enzymes such as myeloperoxidase (MPO), eosinophil peroxidase (EPO) and thyroid peroxidase (TPO) all with similar functions and related structures, especially about the active sites [46]. The activities of the mammalian enzymes are either protective reactions against invasive pathogens, by LPO, EPO and MPO or vital biosynthetic reactions such as thyroxine, T_4, synthesized by TPO.

While the mammalian enzymes and plant peroxidases, such as horseradish peroxidase (HRP), catalyze similar reactions the overall polypeptide structures seem unrelated. The functional relationship between these two genetically unrelated enzyme families is probably due to convergent evolution about the active site [33]. The characterization of a hemeprotein as either a peroxidase or oxygen carrier is not very simple either with a recent report of a hemoglobin with peroxidase activity [9] which incredibly can also break fluorocarbon bonds [35].

LPO serves multiple protective roles. First, as an extrudate in milk, saliva, tears and especially lung surfactant [6] it is a first-line killer of many species of bacteria, fungi and viral agents [18, 41]. Second, because LPO disposes of many invasive microbes by catalyzing the production of $OSCN^-$ from H_2O_2 and SCN^-, it spares the mammal from constantly activating neutrophils to fight infections [17]. These specialized cells act by engulfing the invader then "switch on" MPO and H_2O_2 producing copious amounts of OCl^- and OBr^- which annihilate both invader and neutrophil [12]. Both OCl^- and OBr^- are known mutagens and genotoxic, so if pathogens can be destroyed by the actions of LPO the organism is spared neutrophil activation. LPO is additionally considered the primary means of consuming H_2O_2 in the lungs [11]; LPO in the presence of SCN^- prevents the cell-damaging effects of H_2O_2 including apoptosis [57]. Unfortunately, LPO catalyzes the production of carcinogenic dioxins from chlorophenols in low yields, so the activities of LPO are not entirely harmless [26]. The relationships between structures, functions and physiological implications for the mammalian peroxidases have been recently reviewed [7].

The carbonyl derivatives of hemeproteins have been studied for decades by several methods with justification; CO is both a toxic mimic of dioxygen and nitric oxide, binding at the very same active sites and an important intercellular signal itself in multicellular organisms [36]. In the infrared (IR) radiation region, hemeprotein bound CO exhibits a very strong vibrational absorbance in a region almost devoid of interferences from tissues. The characteristics of the CO absorbance, such as frequency, number of vibrational bands and band width are interpreted as reflecting the stereo- and electronic chemistry at these binding sites. The IR spectra are often highly pH dependent [1] with evidence of a small pH–pD solvent dependence [39, 50], temperature dependence [25], dependence on organic substrate [13] and may even display effects communicated to the CO binding site from a distance of many Ångströms in cystathionine-synthase (CBS) [49]. For these many reasons spectral studies of carbonyl-hemeproteins using both the IR [24] and Resonance Raman (RR) [54] techniques are popular.

The structures from crystallographic studies of *Bos* and *Capra* LPO with a variety of iron ligands including the physiologically important [40, 45] SCN^- in complexes with small, important drugs [43] and inorganic ligands [44] have been previously been reported. Remarkable structural changes occur about the active site including movements of many amino acid residues also involving several molecules of bound water. LPO structure distal to the heme exhibits remarkable flexibility and can even accommodate two SCN^- ligands and several varieties of aspirin based compounds [47]. This protein flexibility even extends down to very low temperatures in glassy, sugar–water solvents [60]. These crystallographic studies have even caught the 3D structure of the product($OSCN^-$) inhibited LPO [45].

Previous reports of the CO vibrational spectra for horseradish peroxidases (HRP), cytochrome c peroxidase (Cyt c PO)and myoglobin (Mb) demonstrated the first order effect of electron density at iron at pH 7 (E_{m7}) on the IR absorbance maxima, ν_{max} and band width at half height $\Delta\nu_{1/2}$ of the C–O stretch by observations and quantum chemical calculations [1, 51]. A clear inverse correlation between the Fe–C absorbance maxima and the iron bound C–O absorbance maxima for both hemeproteins and smaller heme models [32, 55] with support from quantum chemical calculations of model systems and hemeprotein spectroscopy have been reported [58]. While the correlation between $\Delta\nu_{1/2}$ and the Fe(III)/Fe(II) redox potential (E_{m7}) is fairly strict, the correlation between ν_{max} and E_{m7} suffers several exceptions. This makes the ν_{max} an interesting probe for wide variety of secondary effects such as the stereochemistry of the CO binding site and the influences of the proximal ligand, hydrogen bonding and inclusive waters.

We report the structure of crystalline bovine CO–LPO at 2.0Å resolution and contrast with the previously reported cyano–LPO (CN–LPO) structure [40]. The Fe–C–O bond angle of 132° is more acute than other carbonyl hemeproteins in contrast with the electronically related Fe(III), CN–LPO with a more linear Fe–C–N. The orientations of the two ligands are different with the oxygen of CO pointing towards the distal His109 imidazole but the nitrogen of CN is pointing

away. While the relative iron motion is small, the Fe(II) of the CO–LPO is positioned slightly closer to distal His109 than the Fe(III) of the CN–LPO. Likewise for CO–LPO, the distal histidyl residue is favorably situated towards the oxygen for hydrogen bonding while for CN–LPO the distyl His109 placement does not suggest significant hydrogen bonding with the CN^- ligand. In concert with these different structures, the oxygen of Asn437 $O^{\delta 1}$ which is close to the proximal His351 $N^{\delta 1}$ is better positioned to being an H-bond acceptor in CN–LPO rather than in CO–LPO which suggests more imidazolate character for the proximal His351 in the CN–LPO structure.

We also report the IR spectra of the pH dependence of bound CO which are similar to reports for CO–MPO except for a shift of about 13–15 cm^{-1} to higher frequencies both for the unprotonated and protonated forms of CO–LPO. These mammalian peroxidases exhibit IR spectra which are fundamentally different from plant peroxidases in that the v_{max} for the protonated CO is observed at higher frequencies from the unprotonated C–O stretch rather than lower frequencies as for CO–HRP. We suggest the binding sites of CO binding and distal sterochemistry for both LPO and MPO are similar but both are distinct from plant and yeast peroxidases. Our results point to differences of E_{m7}, bound CO v_{max} and activities between LPO and MPO being primarily due to the different hemes within each enzyme. The structure of CO–LPO suggests that orientation of the distal polypeptide, especially the distal histidyl and arginyl residues, is largely responsible for properly positioning a proton at the active sites of mammalian hemeproteins.

2 Materials and Methods

2.1 Protein Purification

Lactoperoxidase was prepared from fresh, un-Pasteurized cow's milk after being skimmed and separated from fat [27, 46]. The purity of LPO was determined by the absorbance ratio of A_{412}/A_{280} (R_Z value) and the R_Z values for the purified LPO were always $\geq$0.93. Lyophilized samples were stored at −20°C or as buffered solutions under liquid nitrogen for further analysis.

2.2 Lactoperoxidase Activity

The activity was determined with excess 2,2′-azino-*bis*-(3-ethylbenzthiazoline-6-sulfonic acid)(ABTS) and H_2O_2 [42] using a PerkinElmer spectrophotometer at 412 nm with one unit of activity defined as the amount of enzyme catalyzing the oxidation of 1μmol of ABTS min^{-1} at 293°K or with excess dicarboxidine and H_2O_2 as the substrates at 440 nm using a Beckman DU7 spectrophotometer [31].

2.3 Crystallization of Lactoperoxidase with Carbon Monoxide

Aliquants of LPO were dissolved in 0.05 M Trizma-HCl buffer (pH 8.0) at a concentration of 30 mg/ml and CO was gently passed through these solutions. Sodium dithionite (2 mM)was added to the protein prior to crystallization to prevent oxidation. A solution with 0.2 M ammonium iodide and 20 % (w/v) PEG-3,350 was separately prepared for the crystallization reservoir. The hanging drop vapor diffusion method with 24-well Limbro plates was used for crystallization and all trials were performed in a glove box filled with carbon monoxide gas. The rectangular-shaped and dark brown colored crystals measuring up to 0.4 × 0.4 × 0.3 mm^3 were obtained after one week.

2.4 X-ray Intensity Data Collection and Processing

The X-ray intensity data were collected using crystals of CO–LPO at the DBT-sponsored Synchrotron beamline BM-14 at the European Synchrotron Radiation Facility (ESRF) in Grenoble (France) on a MAR CCD detector (MAR, USA Inc. Evanston Il). In order to minimize radiation damage the crystal was placed in a nylon loop and kept at 100°K under nitrogen gas during the measurements. Ice formation was avoided by pre-incubation of the crystal for 3 minutes in the reservoir solution containing 22 % w/v PEG-3350. A complete data sets was collected using one crystal. The data were processed and scaled with DENZO and SCALEPACK from the HKL-2000 package [29]. The crystals belong to monoclinic space group P21 with one molecule in the asymmetric unit.

2.5 Structure Determination and Refinement

The structure was determined by the molecular replacement method using the coordinates of LPO as a model (PDB ID: 3GC1) [47]. The rotation, translation functions and rigid body refinements were performed using the data between 12.0 and 4.0Å to yield a clear solution with correlation coefficient of 64 % and an R factor of 35.7 %. The refinement was carried out using program CNS [2]. The (—2Fo–Fc—) and (—Fo–Fc—) maps were calculated to adjust the protein molecule in the electron density using program O [15]. Several cycles of restrained positional refinement with individual B-factors and several rounds of simulated annealing from 3,000 to 300°K allowed the correct tracing of the flexible loops where conformations were markedly different from the initial model. The manual chain tracing was carried out using omit maps across the entire protein chain as the refinement progressed. At the end of this stage, the R_{cryst} and R_{free} factors dropped to values of 0.26 and 0.29 respectively. The Fourier (—2Fo–Fc—) and

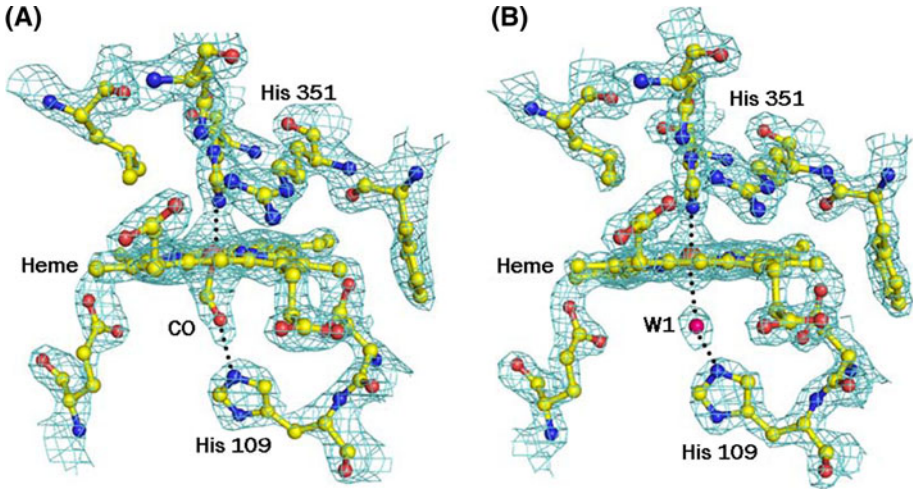


Fig. 1 The $2F_o$–F_c electron density map (contoured at 1σ) for the region around heme moiety as drawn using Pymol. **a** CO–LPO with clear electron density for bound CO. **b** The electron density ($2F_o$–F_c) where water molecule, W1, is observed (PDB ID: 3GC1) at the position of bound CO is shown for comparison. His351 denotes the proximal, iron-bound histidyl residue, His109 denotes the distal histidyl residue which is too far removed to be bonded directly to iron

difference Fourier (—Fo–Fc—) maps computed at this stage showed linearly extended electron density from heme moiety on the distal heme side (Fig. 1a). CO was modeled into this density and the coordinates of carbon and oxygen atoms were included for further refinement. For a comparison electron density from the native structure (PDB ID: 3GC1) with a water molecule at the site corresponding to the above position of carbon monoxide is shown in Fig. 1b. After further cycles of refinement a fresh difference electron density was computed. Using spherical electron densities at 2.5 cut off, the positions of 511 water oxygen atoms were determined. These were also included in the subsequent refinement cycles. The refinement finally converged with R_{cryst} and R_{free} at values of 0.194 and 0.248 respectively. The results of data collection and final refinement statistics are listed in Table 1. The refined atomic coordinates of this complex have been deposited in the Worldwide Protein Data Bank (PDB) with the access code 3V6Q.

2.6 Infrared Measurements

Buffers were made over the pH range from 3.0 to 8.8 using citric acid, sodium phosphate and boric acid all at 50 mM in D_2O and the "pH" adjusted with NaOD solution. D_2O was preferred for IR measurements because the background in the range of 1,880–2,000 cm^{-1} is reduced compared to water; also noted by others [14]. Prior to IR measurements, LPO was concentrated by ultrafiltration under N_2 gas, diluted with deuterated buffer at the desired pH, reconcentrated and the procedure repeated twice. The LPO was concentrated to between 1 and 2 mM in heme, stirred under a stream of scrubbed (chromic perchlorate-amalgamated Zn) CO for 30 min, reduced with the addition of a small amount of fresh dithionite (ICN), then injected into a Beckman-RIIC variable temperature, 0.1 mm IR cell with ZnS windows thermostated at 20°C. CO–LPO integrity was checked after IR analysis by optical spectrophotometry directly through the IR cell. The IR spectra were recorded(15,000 scans) with a Digilab FTS-14C interferometer on single-beam mode at 1 cm^{-1} resolution. Separate spectra of buffer and air were recorded to permit conversion to absorbance and spectra were not smoothed. The IR spectral data were analyzed using the program PeakFit, version 4.12 (SYSTAT), at 1 cm^{-1} resolution. Deconvolution of the CO absorbance into component peaks was performed using the Voight function, which is a combination of Gaussian and Lorentzian peak broadening. Initial estimates were made presuming up to 7 independent CO peaks though only 2 major peaks could be discerned for most spectra.

3 Results

3.1 Overall Structure

The CO–LPO crystals belong to space group $P2_1$ with the unit cell dimensions listed in Table 1. Fig. 1a shows the electron density ($2F_o$–F_c map) with bound C–O while the electron density ($2F_o$–F_c map) in Fig. 1b gives a comparison with a water molecule present at the ligand binding site. The final structure has a resolution of 2.0Å. The entire structure consists of 4,770 protein atoms with residues from 1 to 595, 511 water molecules and one calcium ion. The geometry of the protein molecule is close to ideal values with root-mean-square (RMS) deviations of 0.02Å and 2.1° from the standard values for bond lengths and angles respectively. The overall quality of the model as checked using PROCHECK is good [19]. It shows 90 % of the non-Gly and non-Pro residues in the most favored regions of the Ramachandran plot [34]. The MolProbity score is estimated to be at the 74 percentile [8]. Overall mean B-factor for all atoms is 36.0$Å^2$. Covalently linked CO is observed in the distal heme cavity. One thiocyanate substrate molecule is also observed within the polypeptide distal to

Table 1 Crystallographic data collection and refinement statistics

Data collection	Results
Space group	$P2_1$
Unit cell dimensions (Å)	$a = 54.3$, $b = 80.0$, $c = 76.6$
β(°)	103.0
N subunits per cell	2
V_m (Å^3/Da)	2.3
Solvent content (%)	47.0
Resolution range (Å)	44.13–2.00
Total number measured reflections	677,568
Number unique reflections	42,787
Completeness of data (%)	99.9 (100.0)
R_{sym} (%)	5.0 (36.1)
I/σ (I)	21.0 (2.2)
Refinement	**Results**
R_{crys} (%)	19.4
R_{free} (%) (5 % data)	24.8
Protein atoms	4,770
Calcium ion	1
Heme (1)	43
Water oxygen atoms	511
NAG atoms (4)	56
1,2-Ethanediol (EDO) (2) atoms	8
(4s)-2-Methyl-2,4-pentanediol (MPD) (1) atoms	8
Thiocyanate (1) atoms	3
Iodide	9
Bromide	1
Carbon monoxide	2
RMSD in bond lengths (Å)	0.02
RMSD in bond angles (%)	2.1
RMSD in dihedral angles (%)	19.2
Overall G-factor	−0.20
Average B-factor (Å^2)	
Wilson plot	27.4
Main chain atoms	35.0
Side chains and water molecules	37.0
Overall	36.0
Ramachandran's plot	
Residues in most favored regions (%)	91.0
Residues in additionally allowed regions (%)	8.2
Residues in generously allowed regions (%)	0.8
PDB code	3V6Q

The values in parentheses correspond to the values in the highest resolution shell

heme. The details of the final data processing and refinement parameters are listed in Table 1.

The overall structure of CO–LPO (Fig. 2) is similar to those reported for previously determined LPO structures [40, 43–45, 47, 48]. LPO is a typical hemeprotein with an

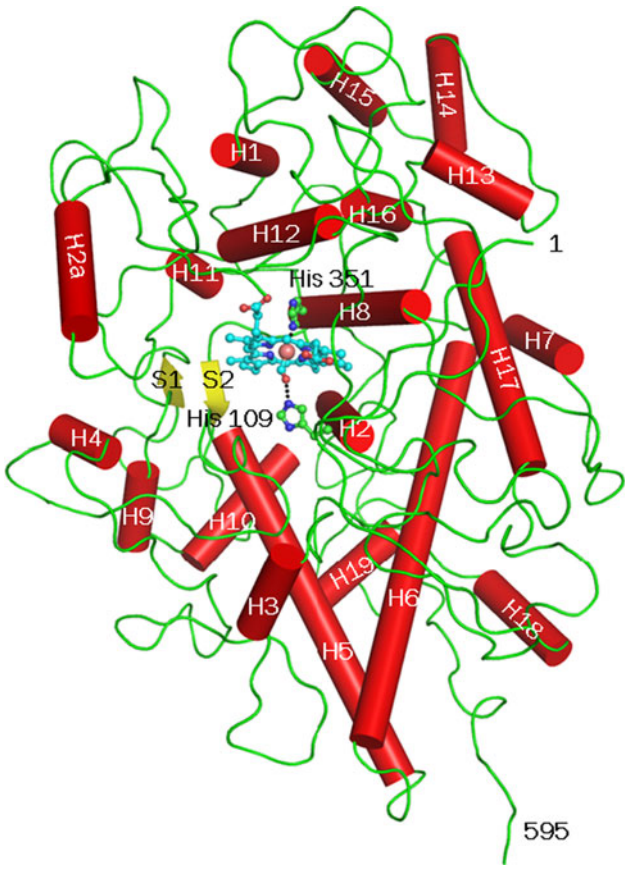


Fig. 2 Overall structure of CO–LPO complex showing the position of CO with carbon atom covalently bonded to the heme iron atom while oxygen atom is hydrogen bonded to His109 $N^{\epsilon 2}$. α-helices are represented as H1–H19 and β-strands are indicated by S1 and S2. The amino terminal of the polypeptide chain is designated as 1 while the last amino acid residue is designated 595. Covalently bound sugars are not shown

abundance of α-helical structure, 33 %, less than 1 % β-sheet and the remaining being random coil. Being a large hemeprotein it has a surface area exposed to water of about 248 nm^2 with portions of 426 amino acids, or 72 %, contacting water.

The values of side chain torsion angles of His109 on the distal side of CO–LPO are $\chi_1 = -80°$ and $\chi_2 = 179°$ while the corresponding values in CN–LPO structure are $\chi_1 = -68°$ and $\chi_2 = 173°$. On the other hand the corresponding values for His351 on the proximal side are $\chi_1 = -57°$ and $\chi_2 = 167°$ for CO–LPO and $\chi_1 = -71°$ and $\chi_2 = 165°$ for CN–LPO.

3.2 Structure Surrounding the Heme

The ligand/substrate binding site on the distal side of the heme moiety is presented in Fig. 3. The CO forms a covalent bond with the iron atom at a distance of 1.73Å with position of carbon atom nearly perpendicular to the heme plane with a porphyrin–Fe–C angle of approximately 85°.

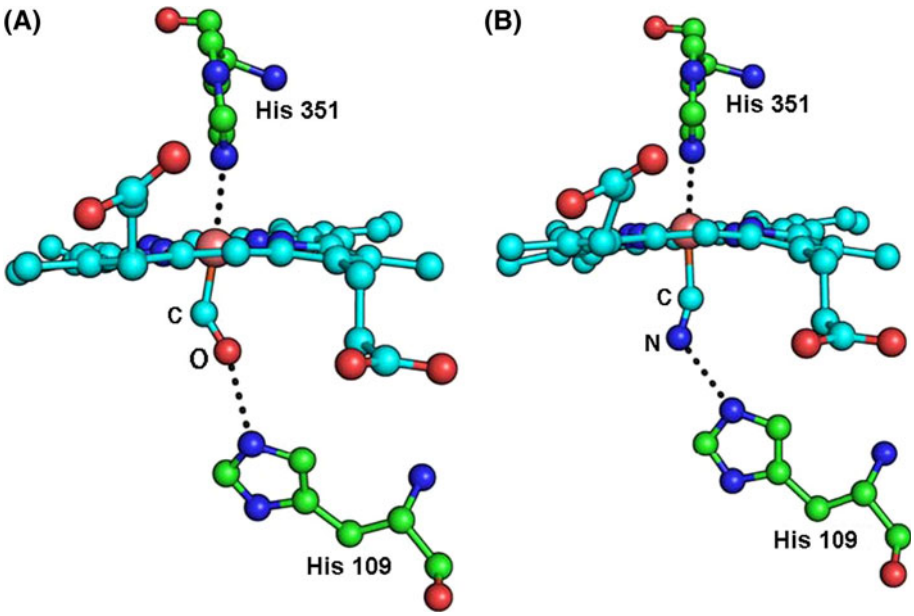


Fig. 3 **a** Interactions of iron(II)-bound CO with distal His109 and proximal His351. **b** Interactions of iron(III)-bound CN with distal His109 and proximal His351

The Fe–C–O bond angle is 132° which is significantly acute compared with other carbonyl hemeproteins where the corresponding angle is generally much closer to 180° [3, 10, 16, 30] with the average value for human HbCO reported from 156° to 180° [37]. The corresponding angle for Fe–C–N in CN–LPO (PDB ID: 3FAQ) is only 161° and in unligated Fe(III) LPO this position is occupied by a water molecule (Fig. 1).

The torsion angle Fe-C-O-$N^{\epsilon 2}$ (His109) is −177.4° while the corresponding torsion angle for Fe--C--N--$N^{\epsilon 2}$ (His109) is −166.6° indicating a nearly planar arrangement between iron atom, CO and His109. The CO bond is parallel, however, to the plane of N1A–N1B–N1C–N1D as the torsion angles are N1A–Fe–C–O of −94.2°, N1B–Fe–C–O of 175.0°, N1C–Fe–C–O of 87.9° and N1D–Fe–C–O of −6.9°. In contrast, for the CN–LPO complex, the position of carbon atom in CN is considerably distorted from planarity as indicated by torsion angle of N1A–Fe–C–N of 40.8°, N1B–Fe–C–N of −44.1°, N1C–Fe–C–N of −140.8° and N1D–Fe–C–N of 137.4°. This shows that the bonding of CO occurs with optimum geometry while CN is considerably distorted. This also shows that the stereochemistry of the active site distal to heme in mammalian peroxidases seems optimally designed for CO and perhaps peroxide but not for CN.

The position of iron atom in CO–LPO is shifted slightly towards CO, while in the case of CN–LPO it has moved towards the proximal side, indicating a stronger Fe–C bond in the CO–LPO structure (Fig. 3). The orientation of the CO unit with respect to distal His109 is favorable for the formation of a hydrogen bond between the oxygen atom and the $N^{\epsilon 2}$ atom of the imidazole ring of His109 while the corresponding hydrogen bond in the structure of CN–LPO

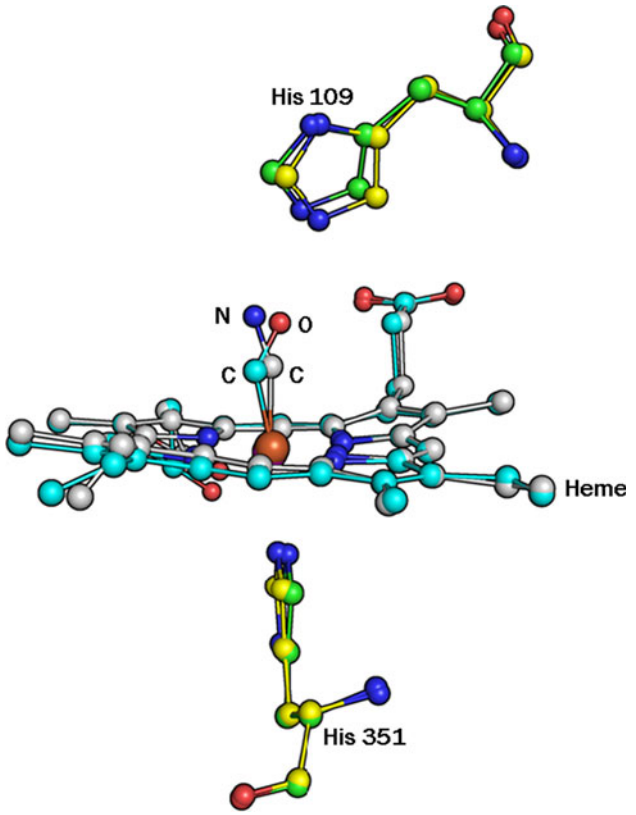


Fig. 4 Superposition highlighting the difference in the orientation of bound CO with respect to bound CN as observed in the structures of CO–LPO and CN–LPO complexes

appears less compatible due to the unfavorable inclination of CN bond with respect to the position of the $N^{\epsilon 2}$ atom as presented in the superimposed structures in Fig. 4. The structures also indicate a degree of flexibility in the side

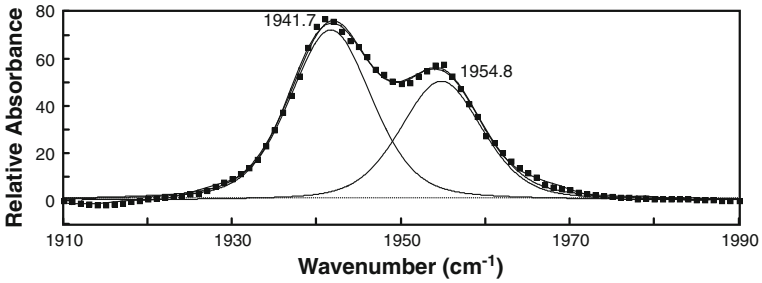


Fig. 5 Infrared spectrum of carbonyl lactoperoxidase at pH 6.0 in deuterated 50 mM sodium phosphate buffer, 1 mM EDTA, displaying computerized resolution into two components. Data pairs used for computerized peak resolution are shown as *squares*

chain of His109 allowing better adjustment with respect to the position of a water molecule, W1, and other residue side chains near this group. The proximal structure of CO–LPO bears resemblance to the proximal structure of MPO with His351 covalently bonded to the iron nearly in the heme plane. A network of hydrogen bonds exists between His351 $N^{\delta 1}$ and Asn437 $O^{\delta 1}$ (2.93Å) and another hydrogen bond between Asn437 $N^{\delta 2}$ and Arg348 NH1 (2.95Å).

3.3 Infrared Results

Figure 5 presents the infrared spectrum of CO–LPO at pD 6.0 in the high frequency region with 2 major absorbances over a wide pD range. One minor, broad band with a maximum at about 1920 cm^{-1} can be detected only at high pD and accounts for only 1–3 % of the CO absorbance. The CO stretch observed here at 1941.7 cm^{-1} is absorbance maximum, ν_{max} for the unprotonated CO, and the maximum at 1954.8 cm^{-1} is the protonated CO stretch. The spectra in all buffers and pD appear similar except the intensities of these two energies. Both absorbances appear non-Gaussian and after baseline normalization, presuming the curves as mixed Gaussian–Lorentz, the CO IR spectra could be resolved into two major stretches by computerized curve fitting (Fig. 5). The ν_{max} energies are not observed to significantly change as a function of pD, averaging 1942.4 and 1954.9 cm^{-1}. The $\Delta\nu_{1/2}$ does vary slightly with pD, from 11.5 to 14.5 cm^{-1} averaging 12.7 cm^{-1} for the unprotonated CO absorbance and 13.8 cm^{-1} for protonated CO, ranging from 11.5 to 17 cm^{-1}. We have previously shown the ν_{max} energy of the unprotonated C–O absorbance to be typically low by about 1 cm^{-1} in D_2O while the ν_{max} energy is low by about 2–3 cm^{-1} for the protonated C–O. This places the unprotonated CO absorbance at $\approx$ 1943.5 cm^{-1} and the protonated CO at $\approx$ 1957.5 cm^{-1} in H_2O. The higher frequency for the protonated CO is reverse of the situation observed for CO–HRP, A2 and C2 [1] but similar to the situation observed for CO–MPO [23].

Figure 6 presents the relative areas of the unprotonated CO IR stretch as the fraction of total CO area with respect to pD. From pD 6 to 8.8 the relative area of the this absorbance is about 60 % of the total area. This decreases to 44 % as the pD is lowered to 3. CO–LPO below this pD

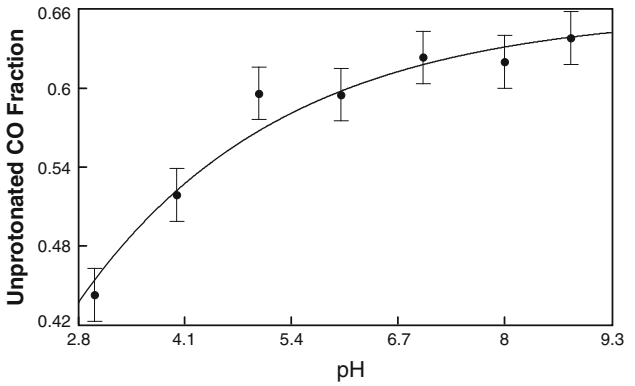


Fig. 6 Fraction of unprotonated CO bound to LPO as a function of pD. Standard errors of area determinations are estimated as 2 %

was not stable in our hands so we cannot guess the lower limit for the unprotonated CO fraction and can only estimate the pK for protonation of the iron-bound CO to $\approx$4, close to the pH 4.5 of maximum turnover for catalysis with H_2O_2 and SCN^- as substrates [4].

4 Discussion

The overall structure for CO–LPO is similar to previously reported structures of LPO and MPO [46]. The distal heme cavity of LPO is connected to the enzyme surface by a wide channel allowing access of a variety of substrates to the heme, such as salicylhydroxamic acid (SHA), benzylhydroxamic acid (BHA) [47], inorganic substrates such as SCN^-, I^- and Br^- as well as six buried waters, while the structure on the proximal side seems more compact [47, 60]. A significant difference between the two heme-proteins is the presence of a unique methionyl–vinyl linkage to heme pyrrole ring A in MPO which is replaced by non-covalent hydrophobic interactions between polypeptide and heme in LPO. This unique structure allows MPO to even catalyze the oxidization of Cl^-.

When comparing the structures of CO–LPO and CN–LPO [40] the ligand binding geometries of the distal sides were observed to be significantly different (Figs. 3 and 4). The Fe–C–N group is nearly linear, bending only slightly in the direction of heme pyrrole rings A and B.

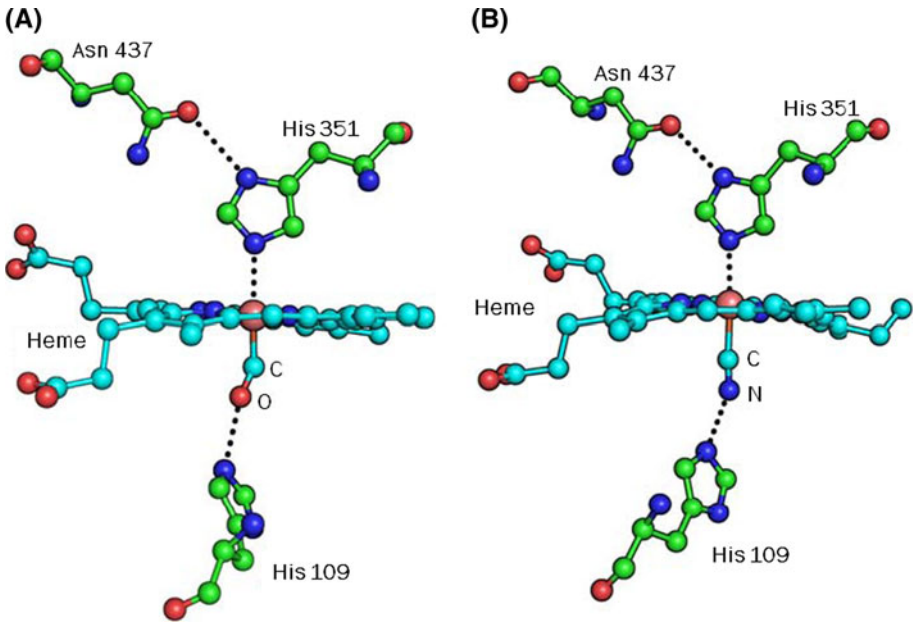


Fig. 7 Comparison of the structure about the heme including proximal H-bonding for CO–LPO at *left* (**a**) and CN–LPO at *right* (**b**)

This suggests little H-bonding interaction between the cyanide N and distal His109 $N^{\epsilon 2}$, and does not agree with a previous prediction for a bent Fe–C–N moiety [14]. The Fe–C–O angle of 132° observed here is far from linear bending towards pyrroles C and D; more bent than reported elsewhere [3, 10, 16, 30]. For instance, much less acute Fe–C–O angles have been reported for bovine and human HbCO of 156°–180° [37], the diheme enzyme MauG of 157° and 171° [59] and sperm whale MbCO of 171° [56]. The arrangement observed here is consistent with a hydrogen bond between His109 and the carbonyl oxygen, also supported by IR data and consistent with previous suggestions of a proton linked to CO binding with LPO [5]. Of course, this unique geometry could be an artifact of crystal packing forces.

On the proximal side His351 $N^{\epsilon 2}$ of helix H_8 is coordinated to the iron atom (2.40Å), while $N^{\delta 1}$ forms a hydrogen bond with Asn437 $O^{\delta 1}$ (2.93Å) from helix H_{12}. The corresponding distances in CN–LPO are shorter and observed as 2.22Å and 2.72Å respectively [40]. These closer alignments are thought to allow enough proton transfer from the imidazole moiety to the Asn that the imidazole acquires a partially negatively charged character which strengthens the iron–ligand bond [21]. This suggestion is supported by the observed "looser" structure here (Fig. 7) and by the IR spectra which are reminiscent to the IR spectra of CO–MPO with a very weak affinity for CO [23].

The IR spectra of these two hemeproteins resemble each other with the protonated CO stretch at higher energies than the unprotonated stretch. Both protonated and unprotonated CO maxima are shifted in parallel to higher energies for CO–LPO by 13–15 cm^{-1} compared to CO–MPO [23]. The IR spectra of CO–MPO and CO–LPO do not resemble the IR spectra of plant peroxidases and myoglobin (Mb) which exhibit protonated CO stretches at lower energy than the unprotonated stretches. Those hemeproteins exhibit spectra with the absorbance of the protonated CO species at lower energies than the unprotonated iron-bound carbonyl [1, 50]. The lower energy of the protonated CO being thought due to electron donation from the oxygen towards the proton, depleting the CO bond of vibrator strength. The unique structural feature of mammalian peroxidases which influence the higher IR frequencies of the protonated CO species is probably the acute Fe–C–O bond angle (132°) observed here in contrast to the more linear Fe–C–O arrangement found in other CO-hemeproteins [3, 10, 16, 22, 30, 53].

5 Speculations

It was previously demonstrated that v_{max} for the unprotonated heme-bound CO is broadly correlated, to the first order, with Em_7. [1, 51] Like many correlations, deviation from the norm is informative and there are several hemeproteins with stretch maxima "off-correlation" and some are presented in Fig. 8. While the v_{max} of CO–LPO at 1943.5 cm^{-1} correlates fairly well with Em_7 this is not true for CO–MPO. The CO stretch at 1927 cm^{-1} is about 17 cm^{-1} lower than predicted suggesting the Fe–C bond might be stronger for CO–MPO than usual for a hemeprotein, but this idea is not supported by CO binding studies suggesting a very weak Fe–C bond [52]. Since the IR spectra for carbonyl mammalian peroxidases share similarities to one another but differ significantly from plant peroxidases one should expect significant differences about the ligand

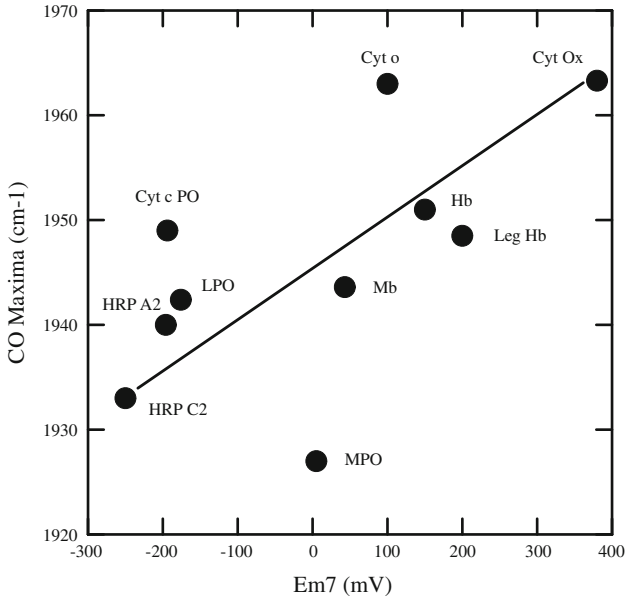


Fig. 8 IR absorbance maxima of unprotonated CO (v_{max}) versus Fe(III)/Fe(II) reduction potentials at pH 7. *Abbreviation key HRP C2* horseradish peroxidase C2, *HRP A2* horseradish peroxidase A2, *LPO* lactoperoxidase, *Cyt c PO* cytochrome c peroxidase, *MPO* myeloperoxidase, *Mb* myoglobin, *Cyt o* cytochrome o, *Hb* hemoglobin, *Leg Hb* soybean legume hemoglobin, *Cyt Ox* cytochrome c oxidase

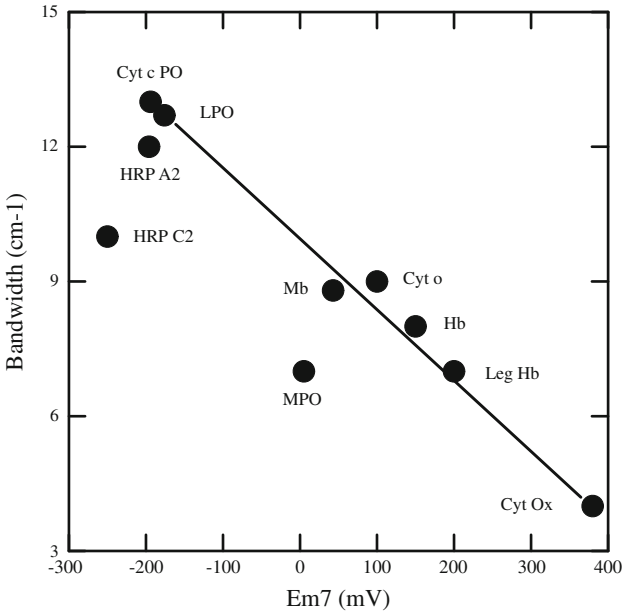


Fig. 9 Width at half maxima of IR absorbance of unprotonated CO ($\Delta v_{1/2}$) versus Fe(III)/Fe(II) reduction potentials [28, 38] at pH 7. *Abbreviation key* same as Fig. 8

binding sites between these protein types. A thorough study of CO affinities and IR spectra for many CO–Mbs with distal single point mutations reveals a major factor governing CO v_{max} is the electrostatic potential contributed by amino acid residues surrounding the bound ligand and not steric hindrance [20]. So to the first order, v_{max} reflects both the heme Em_7 and the electrostatic environment of the ligand pocket.

We think for MPO there are two elements influencing the CO stretch energies and one is a significant imidizolate character to the proximal histidyl–Fe bond [21]. Electron donation from imidazolate to the Fe 3p-orbital would weaken the Fe–C bond but would only marginally influence the C–O vibrator strength which reflects electron donation from the shared CO 2p orbitals back to the Fe 3d levels. The second unique effect is the Fe 3d electronic energies for MPO are heavily influenced by the positive charge from the methionyl–vinyl linkage of heme pyrrole ring A. This allows significant donation from the C–O 2p electrons back to Fe thus lowering the CO stretch to an "abnormal" frequency and strangely weakening CO binding to MPO. One other notable variant from the rough correlation is the CO maxima for CO-cytochrome o suggesting the electronic environment of this bacterial oxidase should be similar to that of mammalian cytochrome c oxidase, despite the different hemes.

There is a strong correlation between CO bandwidth at half maxima ($\Delta v_{1/2}$) for the unprotonated stretch with Em_7, which is updated with Fig. 9 [51]. There are two hemeproteins which do not conform, CO–MPO and CO–HRP C2. We think the deviation for CO–MPO is due to both the electronic withdrawing power of the methionyl–vinyl linkage at heme pyrrole ring A along with a strong proximal His–Fe bond with imidazolate character [23] and for CO–HRP C2 the imidazolate nature of the proximal His–Fe bond, as suggested by others [21]. All other hemeproteins follow this correlation which means, to the first order, that CO bandwidth is due to the electron density at heme iron and not steric events at the CO pocket, which is in agreement with the previous study by Li et al. [20].

So why does MPO have this unique methionyl–vinyl linkage at heme pyrrole ring A and LPO not? We think the cause for this difference ultimately relates to the differing physiological requirements placed on each enzyme. LPO is excreted into poorly controlled environments (lungs, saliva, milk, tears) with the task of occasionally destroying pathogen threats. For this task it must be a tough enzyme—hence the rigid polypeptide proximal to heme. Just as importantly, the potentially destructive nature of activated oxygen must not be allowed to destroy the energetically costly enzyme before the activity can be coupled to a substrate—hence the wide variety of small molecules which are allowed into the flexible active site—any substrate in a pinch. On the other hand MPO exists to be collectively and quickly destroyed, along with the entire neutrophil, in a peroxide burst defending the mammal from a recognized foreign agent which has been caught

trespassing. It is important that MPO turn over active oxygen quickly to create as much OCl^- and OBr^- as possible, hence the methionyl–vinyl linkage which places positive charge in the heme π-cloud destabilizing the oxidized catalytic intermediate enzyme. Such an arrangement would be detrimental to LPO which must stabilize active oxygen with time enough to allow a dilute substrate entrance to the heme to reduce the hemeprotein back to Fe(III) stability.

Acknowledgments Supported in part by financial grants from the Department of Science and Technology (DST) of the Ministry of Science and Technology, New Delhi, India and the Swedish Medical Research Council, B83-3X-6522, B82-13R-6333. MS and SY thank the Council of Scientific and Industrial Research (CSIR), New Delhi for the award of fellowships. TPS thanks Department of Biotechnology (DBT), Ministry of Science and Technology, New Delhi for the award of Distinguished Biotechnology Research Professorship to him.

References

1. Barlow CH, Ohlsson P-I, Paul K-G (1976) Biochemistry 15:2225–2229
2. Brunger AT, Adams PD, Clore GM, DeLano WL, Gros P, Grosse-Kunstleve RW, Jiang JS, Kuszewski J, Nilges M, Pannu NS, Read RJ, Rice LM, Simonson T, Warren GL (1998) Acta Crystallogr D54:905–921
3. Carlsson GH, Nicholls P, Svistunenko D, Berglund GI, Hajdu J (2005) Biochemistry 44:635–642
4. Carlsson J (1983) Biochem Biophys Res Comm 116:568–573
5. Ciaccio C, De Sancis G, Marini S, Sinibaldi F, Santucci R, Arcovito A, Bellelli A, Ghibaudi E, Rose PF, Coletta M (2004) Biophys J 86:448–454
6. Conner GE, Salathe A, Forteza R (2002) Am J Respir Crit Care Med 166:S57–S61
7. Davies M, Hawkins CL, Pattison DI, and Rees MD (2008) Antioxid Redox Signal 10:1199–1234
8. Davis IW, Leaver-Fay A, Chen VB, Block JN, Kapral GJ, Wang X, Murray LW, Arendall WB 3rd, Snoeyink J, Richardson JS, Richardson DC (2007) Nucleic Acids Res 35:W375–W383
9. Du J, Sono M, Dawson JH (2010) Biochemistry 49:6064–6069
10. Edwards SL, Poulos TL (1990) J Biol Chem 265:2588–2595
11. El-Chemaly S, Salathe M, Baier S, Conner GE, Forteza R (2003) Am J Respir Crit Care Med 167:425–430
12. Gűngœr N, Knaapen M, Munnia A, Peluso M, Haenen GR, Chiu RK, Godschalk RWL, van Schooten FJ (2010) Mutagenesis 25:149–154
13. Holzbaur I, English AM, Ismail AA (1996) J Am Chem Soc 118: 3354–3359
14. Hu S, Treat RW, Kincaid JR (1993) Biochemistry 32: 10125–10130
15. Jones TA, Zou JY, Cowan SW, Kjeldgaard M (1991) Acta Crystallogr A47:110–119
16. Kidd RD, Baker HM, Mathews AJ, Brittain T, Baker EN (2001) Protein Sci 10:1739–1749
17. Klebanoff SJ (1991) In: Everse J, Everse KE, Grisham MB (eds) Peroxidases in chemistry and biology, vol 1. CRC Press, Boca Raton, pp 1–35
18. Kussendrager KD, van Hooijdonk AC (2000) Br J Nutr 84(Suppl 1): S19–S25
19. Laskowski RA, Macarthur M, Moss D, Thornton J (1993) J Appl Crystallogr 26:283–290
20. Li T, Quillin ML, Phillips Jr GN, Olson JS (1994) Biochemistry 33:1433–1446
21. La Mar GN, De Ropp JS, Chacko VP, Satterlee JD, Erman JE (1982) Biochim Biophys Acta 708:317–325
22. McMahon MT, de Dios AC, Godbout N, Salzmann R, Kaws DD, Le H, Havlin RH, Oldfield E (1998) J Am Chem Soc 120: 4784–4797
23. Murphy EJ, Marechal A, Sega AW, Rich PR (2010) Biochemistry 49:2150–2158
24. Nienhaus K, Nienhaus GU (2008) Methods Enzymol 437: 347–378
25. Nienhaus K, Nienhaus GU (2011) Biochim Biophys Acta 1814: 1030–1041
26. Oberg LG, Glas B, Swanson SE, Rappe C, Paul K-G (1990) Arch Environ Contam Toxicol 19:930–938
27. Ohlsson PI, Paul K-G (1980) FEBS Lett 110:200–204
28. Ohlsson PI, Paul K-G (1983) Acta Chem Scand B 37:917–921
29. Otwinowski Z, Minor W (1997) Methods Enzymol 276:307–326
30. Park SY, Yokoyama T, Shibayama N, Shiro Y, Tame JR (2006) J Mol Biol 360:690–701
31. Paul K-G, Ohlsson P-I, Jonsson NA (1982) Anal Biochem 124:102–107
32. Paul J, Smith ML, Paul KG (1985) Biochim Biophysi Acta 832: 257–264
33. Poulos TL (2010) Arch Biochem Biophys 500:3–12
34. Ramachandran GN, Sasisekaran V (1968) Adv Protein Chem 23:283–438
35. Roach MP, Chen YP, Woodin SA, Lincoln DE, Lovell CR, Dawson JH (1997) Biochemistry 36:2197–2202
36. Ryter SW, Otterbein LE (2004) Bioessays 26:270–280
37. Safo MK, Abraham DJ (2001) Protein Sci 10:1091–1099
38. Salamon Z, Hazzard JT, Tollin G (1993) Proc Nat Acad Sci 90:6420–6423
39. Satterlee JD, Erman JE (1984) J Am Chem Soc 106:1139–1140
40. Sheikh IA, Singh AK, Singh N, Sinha M, Singh SB, Bhushan A, Kaur P, Srinivasan A, Sharma S, Singh TP (2009) J Biol Chem 284:14849–14856
41. Shin K, Yamauchi K, Teraguchi S, Hayasawa H, Imoto I (2002) J Med Miocrobiol 51:231–237
42. Shindler JS, Bardsley WG (1975) Biochem Biophys Res Commun 67:1307–1312
43. Singh AK, Kumar RP, Pandey N, Singh N, Sinha M, Bhushan A, Kaur P, Sharma S, Singh TP (2010) J Biol Chem 285:1569–1576
44. Singh AK, Pandey N, Sinha M, Kaur P, Sharma S, Singh TP (2011) Biochem Mol Biol 2:328–339
45. Singh AK, Singh N, Sharma S, Shin K, Takase M, Kaur P, Srinivasan A, Singh TP (2009) Biophys J 96:646–654
46. Singh AK, Singh N, Sharma S, Singh SB, Kaur P, Bhushan A, Srinivasan A, Singh TP (2008) J Mol Biol 376:1060–1075
47. Singh AK, Singh N, Sinha M, Bhushan A, Kaur P, Srinivasan A, Sharma S, Singh TP (2009) J Biol Chem 284:20311–20318
48. Singh AK, Singh N, Tiwari A, Sinha M, Kushwaha GS, Kaur P, Srinivasan A, Sharma S, Singh TP (2010) J Biol Inorg Chem 15:1099–1107
49. Singh S, Madzelan P, Stasser J, Weeks CL, Becker D, Spiro G, Penner-Hahn J, Banerjee R (2009) J Inorgan Biochem 103: 689–697
50. Smith ML, Ohlsson PI, Paul K-G (1983) FEBS Lett 163:303–305
51. Smith ML, Paul J, Ohlsson PI, Paul K-G (1984) Biochemistry 23:6776–6785
52. Sono M, Dawson JH, Ikeda-Saito M (1986) Biochim Biophys Acta 873:62–72
53. Spiro TG, Kozlowski PM (2001) Acc Chem Res 34:137–144
54. Spiro TG, Wasbotten IH (2005) J Inorg Biochem 99:34–44

55. Tsubaki M, Ichikawa Y (1985) Biochim Biophys Acta 827: 268–274
56. Vojtechovsky J, Chu K, Berendzen J, Sweet RM, Schlichting I (1999) Biophys J 77:2153–2174
57. Wagner BA, Reszka KA, McCormick ML, Britigan BE, Evig CB, Burns CP (2004) Free Radic Res 38:167–175
58. Xu C, Ibrahim M, Spiro TG (2008) Biochemistry 47:2379–2387
59. Yukl ET, Goblirsch BR, Davidson VL, Wilmot CM (2011) Biochemistry 50:2931–2938
60. Zelent B, Yano T, Ohlsson P-I, Paul J, Smith ML, Vanderkooi J (2005) Biochemistry 44:15953–15959